

2010

Magnetization dynamics triggered by surface acoustic waves

S. Davis

University of Nebraska-Lincoln

A. Baruth

University of Nebraska-Lincoln

Shireen Adenwalla

University of Nebraska-Lincoln, sadenwalla1@unl.edu

Follow this and additional works at: <http://digitalcommons.unl.edu/physicsadenwalla>

Davis, S.; Baruth, A.; and Adenwalla, Shireen, "Magnetization dynamics triggered by surface acoustic waves" (2010). *Shireen Adenwalla Papers*. 20.

<http://digitalcommons.unl.edu/physicsadenwalla/20>

This Article is brought to you for free and open access by the Research Papers in Physics and Astronomy at DigitalCommons@University of Nebraska - Lincoln. It has been accepted for inclusion in Shireen Adenwalla Papers by an authorized administrator of DigitalCommons@University of Nebraska - Lincoln.

Magnetization dynamics triggered by surface acoustic waves

S. Davis, A. Baruth,^{a)} and S. Adenwalla^{b)}

Department of Physics and Astronomy and the Nebraska Center for Materials and Nanoscience,
University of Nebraska-Lincoln, Lincoln, Nebraska 68588-0299, USA

(Received 14 October 2010; accepted 2 November 2010; published online 7 December 2010)

Investigations into fast magnetization switching are of both fundamental and technological interest. Here we present a low-power, remote method for strain driven magnetization switching. A surface acoustic wave propagates across an array of ferromagnetic elements, and the resultant strain switches the magnetization from the easy axis into the hard axis direction. Investigations as a function of applied magnetic field as well as unidirectional anisotropy (the exchange bias) reveal excellent agreement with prediction, confirming the viability of this method. © 2010 American Institute of Physics. [doi:10.1063/1.3521289]

Fast magnetization dynamics, on time scales of ~ 100 ps, entail a complex interplay between angular momentum and energy reservoirs, electron-phonon coupling, and the precession modes available, presenting an array of noteworthy fundamental questions, in addition to the obvious applications in magnetic memories. The answer to the question “How fast can the magnetization switch?” depends on the mode of reversal, the method(s) used to initiate the reversal, as well as the size, shape, and material properties of the ferromagnet, and has been investigated using short pulsed magnetic fields,¹ light pulses,² and thermal excitations³ in pump-probe type experiments, with the fastest magnetization reversal occurring at a time scale of 30 ps.³

The interplay between magnetization and strain, arising from the spin-orbit interaction,⁴ is governed by the magnitude of the magnetostrictive coefficient.⁵ In a recent experiment,⁶ short light pulses excite picosecond acoustic waves, resulting in fast magnetization changes in a thin film of (Ga,Mn)As.⁶ Here we exploit the sensitivity of the magnetization direction to strain to study an efficient, low-power, and low cost method for fast magnetic switching using a strain coupled device that rotates the magnetization between the hard and easy axes at the resonant frequency (91 MHz) of a surface acoustic wave (SAW) transducer⁷ providing directional, time dependent strain to a micron scale array of Co bars. Previous experiments have shown changes in the SAW propagation through continuous magnetic thin films of Ni and permalloy with magnetization direction.^{8–11}

The sample [Fig. 1(a)] is produced using magnetron sputtering and optical lithography with a wet etch process and consists of two interdigitated titanium transducers (IDTs) of 100 fingers on a Y-Z cut LiNbO₃ substrate. The finger spacing and width are both 10 μm , resulting in a SAW wavelength of 40 μm . Frequency sweeps show the expected resonances, based on the known SAW velocity in the z-direction, with a room temperature fundamental mode at 91.75 MHz, a Q value of 127 [Figs. 1(b) and 1(c)], as well as all the odd harmonics up to $n=7$ at 643 MHz. The low temperature resonance shift [Fig. 1(b)] results from the temperature dependence of the SAW velocity and wavelength. Tem-

perature dependent data are taken at the appropriate resonant frequency. Between the two IDTs is an array of 10 nm thick Co bars, each 10 μm wide and 40 μm long, with a center-to-center spacing that is commensurate with the SAW wavelength of 40 μm . This ensures that each element of the array experiences the same strain at a given time, enabling spatial signal averaging. The bars are aligned such that the long axes lie along the y-axis of the LiNbO₃. The chosen crystalline cut and propagation direction (z-axis of the LiNbO₃) ensure that the maximum strain amplitude is in the direction of propagation, stretching and compressing the magnetic elements along the short hard axis direction. The application of sufficient strain along this direction will switch the magnetization from the long easy axis direction into the short hard axis direction at the frequency of SAW excitation. Magnetization components along the y and z directions are measured using the magneto-optical Kerr effect (MOKE) in a Janis displex with optical windows for low temperature measurements.

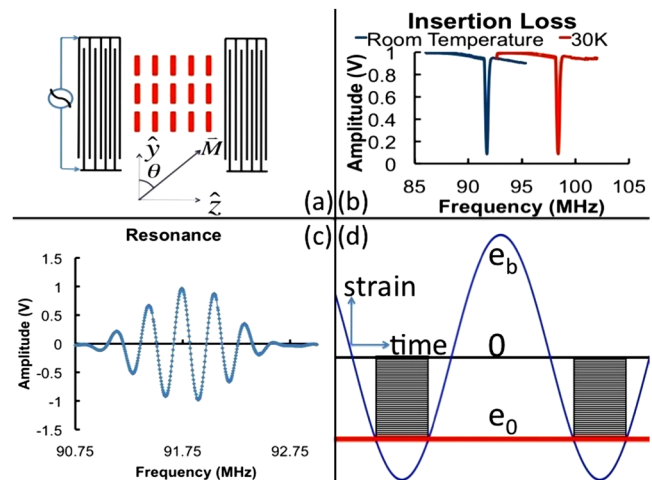


FIG. 1. (Color online) (a) SAW device with 40 $\mu\text{m} \times 10 \mu\text{m}$ Co rectangles spaced by the 40 μm wavelength of the SAW. (b) Temperature dependence of the resonance observed via insertion loss at room temperature and 30 K. (c) Fundamental resonance at 91.75 MHz measured via transmission across the two IDTs at room temperature using frequency modulation. (d) Time dependence of the magnetization at zero applied field. e_0 is the minimum strain required to switch the magnetization into the hard axis direction. For a strain wave of amplitude e_b , where $e_b > e_0$, the magnetization switches into the hard axis direction for the time period represented by the hatched rectangles.

^{a)}Present address: University of Minnesota-Twin Cities.

^{b)}Author to whom correspondence should be addressed. Electronic mail: sadenwalla1@unl.edu.

MOKE measurements at room temperature along the easy and hard directions show the expected shape anisotropy, for which calculations give $K_s = 6.2 \times 10^2 \text{ J/m}^3$, assuming the bulk magnetization of Co.

The free energy for a single Co bar, assuming single domain coherent processes, is⁵

$$E = -\mu_0 M_s H \cos \theta - K_s \cos^2 \theta - K_{EB} \cos \theta + B_1 e_{33} \sin^2 \theta, \quad (1)$$

where the first three terms are the Zeeman energy, shape anisotropy, and the unidirectional anisotropy (exchange bias) terms, respectively. The unidirectional anisotropy arises from the naturally occurring CoO film on the uncapped Co bars resulting in a blocking temperature of 105 K. The last term is the strain energy where B_1 is the magneto-elastic (ME) coefficient for Co, e_{33} is the strain along the short z-axis, and θ is the angle between the magnetization vector and easy axis. In this convention, a negative value of $B_1 e_{33}$ lowers the energy along the hard axis direction.⁵ Since B_1 for bulk Co is positive ($6 \times 10^6 \text{ N/m}^2$), only compressive strain will lead to rotation of the magnetization.

Minimization of the free energy with respect to θ results in the minimum compressive strain at which the magnetization will move away from the easy axis direction,

$$e_{33} > \left| \frac{(\mu_0 M_s H + K_{EB} + 2K_s)}{2B_1} \right|. \quad (2)$$

Although MOKE measurements at the driving frequency of the transducers would appear to be the logical choice to measure the magnetization switching, in common with all piezoelectric materials, LiNbO_3 is electro-optically active with a large electro-optical coefficient.¹² The electric field induced changes in the refractive index lead to changes in the MOKE signal that are independent of the magnetization. DC MOKE, averaged over multiple cycles, effectively eliminates this effect since the electro-optic coefficient is linear with electric field. At room temperature, with $H=0$, only two stable states exist, with M pointing either along the long easy axis direction or the short hard axis direction. Hence, the magnetization response to a sinusoidally driven IDT will be a square wave, as shown in Fig. 1(d). If the amplitude of the strain wave e_1 is less than the threshold strain e_0 [Eq. (2)], the magnetization remains along the easy axis direction, switching to the hard axis occurs only when the threshold strain is exceeded. For a material with a positive ME coefficient, this will occur over some fraction of the negative (compressive) half of the cycle. During the other portion of the cycle, the magnetization is pinned along the long easy axis. There exists a net dc component of M along the hard axis direction, corresponding to the average signal $M_s \Delta t / T$, where M_s is the saturation magnetization, Δt is the time interval over which the magnetization remains along the hard axis, and T is the period of the strain excitation given by

$$M_s \frac{\Delta t}{T} = \frac{\pi - 2 \sin^{-1}(e_1/e_0)}{2\pi}. \quad (3)$$

dc measurements of the magnetization along the hard axis as a function of driving voltage of the IDT have a characteristic signature: (i) a threshold voltage, $e_0 = e_1$, below which there is no component of magnetization along the in-plane hard axis direction, followed by (ii) a subsequent in-

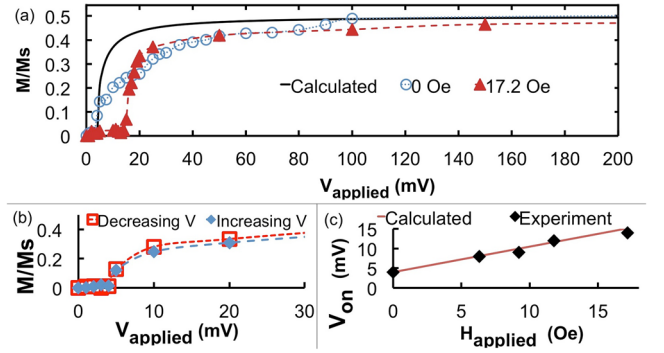


FIG. 2. (Color online) (a) Hard axis magnetization signal as a function of applied voltage, normalized to the saturation magnetization along the hard axis direction at easy axis applied fields of $H=0$ Oe and at $H=17.2$ Oe. The dashed lines are guides to the eye. The solid line is the expected zero field behavior from Eq. (3). (b) Reversibility of magnetization signal with increasing and decreasing voltage. (c) Turn-on voltage as a function of applied field along the easy axis (symbols) together with the expected slope (solid line) calculated from the free energy minimization.

crease in the dc magnetization signal with increased driving voltage, asymptotically approaching a value of $M_s/2$. This precise behavior is observed in hard axis dc MOKE measurements in Fig. 2(a). After saturation along the easy axis, the external magnetic field is turned off and the MOKE signal along the short in-plane hard axis is measured as a function of applied voltage, indicating a turn-on voltage of 4.5 mV and the approach to saturation at about 100 mV. When the excitation voltage is turned off and a magnetic field of 1200 Oe is applied to saturate the magnetization along the hard axis direction, the resulting change in MOKE signal is exactly twice that at the highest driving voltage, indicating both qualitative and quantitative agreement with the expected behavior. Note that there must exist a small symmetry breaking field (probably caused by a slight misalignment of the initial saturating magnetic field) to ensure that the magnetization switches preferentially to one of the two equivalent hard axis directions. Identical measurements on a bare LiNbO_3 region reveal no changes in the MOKE signal during excitation.

The calculated threshold voltage, assuming the bulk ME coefficient for Co, is 16 mV, higher than the experimental 4.5 mV obtained. However, the ME coefficients of thin films are sensitively dependent on both the thickness and the coupling to the substrate and may be 3–5 times larger than in the bulk.¹³ From our data, we calculate a ME coefficient of $1.83 \times 10^7 \text{ N/m}^2$ for 10 nm thick Co bars grown on LiNbO_3 .

Similar behavior with a slightly higher turn-on voltage has been seen for the highest driving frequency of 643 MHz, an effect attributed to the reduced efficiency of the higher harmonic modes. The strain dependence of the dc hard axis magnetization, given by Eq. (3) and plotted as the solid line in Fig. 2(a), indicates that the data show a much slower approach to saturation than expected, which one might attribute to regions of domains resistant to rotation into the hard axis direction. However, the reversibility of the effect with increasing and decreasing voltage, shown in Fig. 2(b), indicates that this is not a major issue, and the slow approach to saturation is not fully understood.

At room temperature, the exchange bias is zero, and in the presence of an externally applied field along the easy axis direction, energy minimization and the stability condition indicate that the magnetization rotates continuously from the

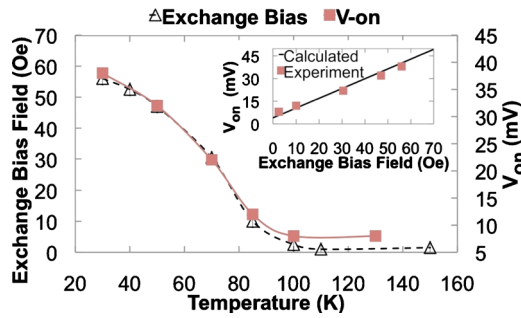


FIG. 3. (Color online) Exchange bias vs temperature (open triangles, left axis) and turn-on voltage (squares, right axis) vs temperature. The inset shows the turn-on voltage as a function of exchange bias (squares) together with the expected linear dependence (solid line) calculated from free energy minimization.

easy y-axis direction into the hard z-axis direction, with an angle given by $\cos \theta = -\mu_0 M_s H / [2(K_s + B_1 e_{33})]$. MOKE measurements of the M_z component of magnetization as a function of driving strain (i.e., applied voltage) and applied field show a linear increase of the turn-on voltage with increasing applied field along the easy axis direction, as shown in Fig. 2(c). The solid line in Fig. 2(c) is the expected dependence from Eq. (2), with the slope given by $M_s / 2B_1$, where we use the value of B_1 obtained from the 0 field turn-on voltage. Our data show excellent quantitative agreement with the expected dependence.

The naturally occurring CoO layer formed *ex situ* allowed an investigation of the effects of exchange bias on the strain driven switching. Over the temperature range from room temperature to 100 K, the turn-on voltage shows a small, almost linear, increase (from 4.5 to 6 mV) at zero applied field, resulting from the linear decrease in the piezoelectric coefficient of LiNbO_3 with temperature.¹² Just below the blocking temperature of 105 K there is a dramatic increase in the turn-on voltage, which we ascribe to the non-zero exchange bias term in the free energy. The exchange bias acts to pin the magnetization along the easy axis direction, increasing the threshold voltage for rotation of the magnetization away from the easy axis, as given by Eq. (2), with the applied field $H=0$. A plot of the exchange bias field and the turn-on voltage as a function of temperature indicates an exact correlation between the two. The turn-on voltage at 30 K, where the exchange bias field is 56 Oe, is 38 mV, a factor of 6 increase. The turn-on voltage as a function of the exchange bias field is plotted in Fig. 3(b), together with the

expected slope, $M_s / 2B_1$, showing excellent agreement.

In conclusion, dc MOKE measurements of the strain driven magnetization switching of a Co bar array show excellent quantitative agreement with the expected behavior based on free energy considerations, implying that strain triggered magnetization rotation is a viable method for producing large ($\pi/2$) changes in the magnetization direction. The data presented here investigate relatively slow switching, on time scales of 10 ns. SAW transducers operating at much higher frequencies (~ 10 GHz) are readily available⁷ and, at these high frequencies, approach time scales that are close to fundamental limits in magnetization dynamics, leading to observable lag times in the magnetization response to the driving strain wave.

This research is supported by the NSF through the Materials Research Science and Engineering Center program Grant No. DMR-0820521. Funding for S.D. was provided by an Undergraduate Creative Activities and Research Experiences (UCARE) grant from UNL. Parts of this work were carried out in the University of Minnesota Nanofabrication Center, which receives partial support from NSF through the NNIN program. We acknowledge J. A. Claes' help with the photomask drawings.

¹C. H. Back, D. Weller, J. Heidmann, D. Mauri, D. Guarisco, E. L. Garwin, and H. C. Siegmann, *Phys. Rev. Lett.* **81**, 3251 (1998).

²J.-Y. Bigot, M. Vomir, and E. Beaurepaire, *Nat. Phys.* **5**, 515 (2009).

³K. Vahaplar, A. M. Kalashnikova, A. V. Kimel, D. Hinzke, U. Nowak, R. Chantrell, A. Tsukamoto, A. Itoh, A. Kirilyuk, and Th. Rasing, *Phys. Rev. Lett.* **103**, 117201 (2009).

⁴D. Sander, *Rep. Prog. Phys.* **62**, 809 (1999), and references therein.

⁵R. C. O'Handley, *Modern Magnetic Materials, Principles and Applications* (Wiley, New York, 2000).

⁶A. V. Scherbakov, A. S. Salasyuk, A. V. Akimov, X. Liu, M. Bombeck, C. Brüggenmann, D. R. Yakovlev, V. F. Sapega, J. K. Furdyna, and M. Bayer, *Phys. Rev. Lett.* **105**, 117204 (2010).

⁷C. K. Campbell, *Surface Acoustic Wave Devices for Mobile and Wireless Communications* (Academic, Boston, 1998).

⁸C. Krischer, I. Feng, J. B. Block, and M. Levy, *Appl. Phys. Lett.* **29**, 76 (1976).

⁹I. Feng, M. Tachiki, C. Krischer, and M. Levy, *J. Appl. Phys.* **53**, 177 (1982).

¹⁰M. Levy and H. Yoshida, *J. Magn. Magn. Mater.* **35**, 139 (1983).

¹¹D. Walikainen, R. F. Wiegert, and M. Levy, *J. Appl. Phys.* **63**, 3927 (1988).

¹²R. S. Weis and T. K. Gaylord, *Appl. Phys. A: Mater. Sci. Process.* **37**, 191 (1985).

¹³O. Song, C. A. Ballentine, and R. C. O'Handley, *Appl. Phys. Lett.* **64**, 2593 (1994).